Pr-rich cerium-zirconium-praseodymium mixed oxides for automotive exhaust emission control

Simon Fahed, Rémy Pointecouteau, Mimoun Aouine, Antoinette Boreave, Sonia Gil, Valérie Meille, Philippe Bazin, Olivier Toulemonde, Alain Demourgues, Marco Daturi, et al.

Pr-rich cerium-zirconium-praseodymium mixed oxides for automotive exhaust emission control

Simon Fahed[a,b], Rémy Pointecouteau[c,d], Mimoun Aouine[a], Antoinette Boréave[a], Sonia Gil[a], Valérie Meille[a], Philippe Bazin[b], Olivier Toulemonde[c], Alain Demourgues[c], Marco Daturi[b], Philippe Vernoux[a,*]

[a] *Univ Lyon, Université Claude Bernard Lyon 1, CNRS, IRCELYON, F-69626, Villeurbanne, France*

[b] *Normandie Université, ENSICAEN, UNICAEN, CNRS, Laboratoire Catalyse et Spectrochimie, 14050 Caen, France*

[c] *CNRS, Université de Bordeaux, ICMCB, 87 Avenue du Dr. Albert Schweitzer, 33608 Pessac, France*

[d] *Institut de Chimie des Milieux et Matériaux de Poitiers (IC2MP), University of Poitiers, CNRS UMR 7285, TSA51106 – F86073 Poitiers Cedex 9, France*

*to whom correspondence should be addressed:

Tel.: +33 472431587

E-mail: philippe.vernoux@ircelyon.univ-lyon1.fr

Abstract

This study describes the textural, structural, redox properties, oxygen reactivity of two Pr-rich cerium-zirconium-praseodymium (CZP) oxides ($Ce_{0.45}Zr_{0.10}Pr_{0.45}O_{2-x}$ and $Ce_{0.475}Zr_{0.05}Pr_{0.475}O_{2-x}$) and their catalytic activity for propane and CO oxidation in both stoichiometric and lean conditions, two important reactions for automotive exhaust emission control. The concentration of oxygen vacancies can be tuned by the quantity of Pr^{3+} cations which depend both on the preparation method and the composition. The $Pr^{4+}(4f^1)/Pr^{3+}(4f^2)$ ratio was accurately determined by magnetic measurement. A highly energetic grinding step was found to double this Pr^{3+} concentration, resulting in a strong enhancement of the low-temperature reducibility, bulk oxygen mobility and catalytic activity for propane deep oxidation. Pr-rich CZP oxides seem to be less relevant for CO oxidation, which is mainly driven by the specific surface areas. These Pr-rich CZP mixed oxides present better performances for lean conditions, suggesting their possible role in diesel oxidation catalysts applications.

Keywords: mixed metal oxides; emission abatement; automotive exhaust control; TWC; oxidation catalysts.

1. Introduction

Ceria-based oxides have a pivotal role in heterogenous catalysis [1,2]. The Ce^{4+}/Ce^{3+} redox couple confers to these oxides relevant properties for catalysis such as a high oxygen storage capacity (OSC) combined with reactive lattice oxygen. Ceria doped with isovalent Zr^{4+} cations forms a solid solution that improves the thermal stability, the reducibility of Ce^{4+} cations and the OSC. The main application of these mixed oxides concerns the vehicles emission control as ceria-zirconia (CZ) enters into the composition of three-way converters (TWC), commonly used to remove unburnt hydrocarbons, CO and NO_x in the exhaust of gasoline engines. Ceria-based oxides are also intensively investigated for catalytic soot oxidation to regenerate diesel and gasoline particulate filters and for many other reactions like water-gas shift, reforming, selective oxidation or oxidative [1,3,4]. Even if CZ mixed oxides are industrially applied, they are not used as active catalytic phases, but mainly as supports to disperse noble metal nanoparticles and optimize their catalytic activity. The drastic decrease of PGM (Pt Group Metal) loadings in the catalyst formulation is required to develop sustainable processes and to reduce cost. To achieve this objective, the redox and catalytic properties of CZ mixed oxides have to be further improved for, on one hand optimizing metal/support interaction at mid-term and, on the other hand, being active without PGM at long-term. To boost the catalytic properties of CZ oxides, two strategies are reported in the literature. The first one deals with the development of well-controlled preparation methods to optimize the texture and the morphology of nano-ceria such as the type of exposed crystal plans [5]. The second route is intended to tailor the CZ composition with the introduction of other elements with variable oxidation state. Among all the different investigated dopants, Pr is of great interest as, with this reducible element, the two Pr^{3+} and Pr^{4+} valence states can co-exist in a CZ solid solution even in oxidizing conditions at high temperature. This mixed

valence state of Pr cations offers many advantages like improving the reducibility, the concentration of oxygen vacancies, which can be mobile in the network and then the OSC values. For instance, Abel et al. [5] have explored the structural and redox properties of $Pr_{1-x}Zr_xO_{2-y}$ ($0 \leq x \leq 1$) solid solutions and found that the Pr^{3+} rate in the mixed oxide increases with the Zr content since short Zr^{4+}— O^{2-} bonds can compensate larger Pr^{3+} — O^{2-} ones in the network.

Several studies [2,6] evidenced the fast and reversible oxygen uptake and evolution, as well as a high reducibility of a Pr rich CP oxide ($Pr_{0.55}Ce_{0.45}O_{2-x}$). More recently [7], a similar equimolar CP composition ($Ce_{0.5}Pr_{0.5}O_{2-x}$) was found to present the highest OSC, oxygen bulk mobility and the greatest catalytic activity for soot oxidation among a series of $Ce_{1-x}Pr_xO_{2-y}$ (x = 0, 0.1, 0.25, 0.5). Such good catalytic properties of Pr rich CP oxides for oxidation reactions are described in the literature for NO oxidation [8–10], NO_x-assisted soot oxidation [8,10], soot, CO, methane, ethylene, propylene and 1-2-dichloroethane combustion [11–15]. All these Pr rich CP oxides are p-type semiconductors [15], stabilizing O^- ionic species on their surface, which are quite effective for oxidation reactions and especially oxygen mobility assisted by $Pr^{4+}(4f^1) + O^{2-}(2p^6) \Leftrightarrow Pr^{3+}(4f^2) + O^-(2p^5)$ [16] charge transfer equilibrium. Furthermore, many studies have observed a surface Pr enrichment versus the nominal bulk CP composition, which could amplify the beneficial impact of Pr on the catalytic properties. This Pr enrichment on the surface and at the domain boundaries increases with the calcination temperature and the Pr content [12,17]. This makes Pr rich CP oxides promising catalysts for oxidation reactions. Unfortunately, their thermal stability is weak and low surface areas are reported for oxides calcined at temperature above 700 °C [6,9,18,19]. On another hand, zirconium- praseodymium (ZP) mixed oxides supporting Pd also present interesting properties for exhaust emissions oxidation without the formation of secondary pollutants such as noxious species [20].

Pr rich cerium-zirconium-praseodymium (CZP) mixed oxides could combine the promising properties of Pr rich CP or ZP with the thermal stability of CZ materials. For instance, Rossignol et al. [19] have shown that the surface area after a calcination at 900 °C of $Ce_{0.45}Zr_{0.1}Pr_{0.45}O_{2-x}$ is much higher than that of the equimolar CP oxide (20 vs. 4 m^2/g), highlighting the beneficial role of Zr in the thermal stability. Furthermore, this CZP compound exhibited the highest OSC. More recently, we found that a mixed oxide with the same composition exhibits a very high reducibility and electrical conductivity, as already observed for Pr rich CP oxides [16]. Furthermore, magnetic measurements have confirmed that high Pr^{3+} rates can be stabilized in air in CZP solid solutions [16], which can reach 56% for Zr-rich composition like $Ce_{0.33}Zr_{0.33}Pr_{0.33}O_{2-x}$. The electronic conductivity is mainly associated with electron exchange between Pr^{3+} and Pr^{4+} cations [21]. The remarkable electrical property of Pr rich CZP is supposed to promote the surface oxygen exchange reaction as it is accompanied by a counter flow of electrons towards the surface.

Nevertheless, to the best of our knowledge, the catalytic performances of Pr rich CZP mixed oxides are not reported in the literature. Only a few studies have described the activity of Pr poor CZP materials containing atomic Pr loading lower than 11% for CO and soot oxidation [22–24]

This study describes the textural, structural, redox properties and oxygen reactivity of two Pr rich CZP oxides ($Ce_{0.45}Zr_{0.10}Pr_{0.45}O_{2-x}$ and $Ce_{0.475}Zr_{0.05}Pr_{0.475}O_{2-x}$) as well as their catalytic activity for CO and propane oxidation in both stoichiometric and lean conditions. We have selected these two reactions as CO and propane are two pollutants present in the exhaust of gasoline and Diesel vehicles. These two oxidation reactions are supposed to proceed via a Mars and Van Krevelen (MvK) mechanism which involves lattice oxygen species of the catalyst. Therefore, these two reactions are particularly suitable with redox oxides with a high oxygen bulk mobility like CZP. Furthermore, propane and CO exhibit opposite chemisorptive

properties on a surface, CO being easily adsorbed via electrons transfer while propane is tricky to activate due the energy demanding cleavage of the first C-H bond.

Their Pr^{3+} concentration was estimated by magnetic measurements and methanol adsorption recorded by FTIR, aiming to evaluate its impact on the catalytic properties. For comparison, a CZ mixed oxide ($Ce_{0.70}Zr_{0.30}O_2$) and a Pr poor CZP compound ($Ce_{0.62}Zr_{0.30}Pr_{0.08}O_2$) were also synthetized and characterized.

2. Experimental

2.1. Synthesis

Pr-doped CZ oxides have been prepared by the coprecipitation method [16] from nitrate precursors in basic medium (pH = 10) and calcined in static air at 600 °C for 12 h. A CZ mixed oxide was also prepared for comparative purposes by using the same method. Between the coprecipitation process and the annealing at high temperatures in oven, maturation step under air (4h) at room temperature and finally several washing/centrifugation using diluted ammonia (M/1000) followed by drying in ethanol at T= 50°C during one night, allow getting pure phases with sufficient surface area after calcination under air. The nomenclature of the prepared oxides (Table 1) refers to their cationic composition and their Pr content, e.g. CZP45 for 45 molar % Pr, 45 molar % Ce and 10 molar% Zr. Table 1 gives the list of prepared oxides, their nomenclature and their nominal composition. After the calcination step, all samples were grinded with a mixer-mill (MM-200-Retsch) in a ball-mortar containing two zirconia balls of 5 mm diameter at 10 Hz for 6 h. Raw powders contained large grains with a bimodal distribution centred at around 40-60 µm and 180-240 µm (Fig. S1). After grinding, the granulometry becomes monomodal with a d50 lower than 10 µm (Fig. S1, Table 1).

Table 1. Nomenclature of the grinded catalysts, composition and granulometry.

Composition	Name	d50 (µm)	at. % from ICP		
			Ce	Zr	Pr
$Ce_{0.70}Zr_{0.30}O_{2-x}$	CZ	7	72.4	27.6	-
$Ce_{0.62}Zr_{0.30}Pr_{0.08}O_{2-x}$	CZP8	7	64.2	27.6	8.2
$Ce_{0.45}Zr_{0.10}Pr_{0.45}O_{2-x}$	CZP45-LS*	5	45.5	9.3	45.2
$Ce_{0.475}Zr_{0.05}Pr_{0.475}O_{2-x}$	CZP47	10	48.7	4.6	46.7
$Ce_{0.45}Zr_{0.10}Pr_{0.45}O_{2-x}$	CZP45-HS*	5	45.4	9.4	45.1

*LS for low specific surface area and HS for high specific surface area

2.2. Catalysts characterisation

The content of Ce, Zr and Pr in the oxides was quantified by inductively coupled plasma emission spectroscopy (ICP-OES) in an Activa spectrometer from Horiba. N_2 adsorption-desorption at -196 °C was performed on a Tristar instrument from Micromeritics. Before the measurement, the samples were degassed at 300 °C overnight under vacuum (10^{-5} bar). The specific surface area (SSA) of each sample was obtained by the Brunauer-Emmett-Teller (BET) method while the mean pore size diameter was calculated by the Barrett-Joyner-Halenda (BJH) method applied to the desorption curve. The X-ray diffraction pattern of all samples was recorded at room temperature using X-ray powder diffractometer Bruker D8 Advance A25 with CuKα1,2 average radiation (λ = 0.15418 nm) in a wide range of Bragg angles 2θ (20–80°) with a step of 0.020° and a counting time of 100 s. The XRD whole powder pattern decomposition were performed using Le-Bail method (Jana 2006) with conventional reliability factors. The unit cell and profile parameters used to determine the average crystallite size were refined.

The granulometry of the samples was measured with a Mastersizer S Granulometer (Malvern Instrument) from around 40 mg of the mixed oxides in deionised water suspension.

The Curie constants (C) and Weiss temperatures (θp) were deduced from magnetic susceptibility measurements with the magnetizations being recorded between 125 and 300 K (speed rate: 10°/min) in ambient air in a magnetic field of 18 000 Oe. Magnetic measurements were performed on a MicroSense EZ7 vibrating magnetometer. We quantified the Pr^{4+}/Pr^{3+}

ratios considering that cerium cations are only stabilised as 4+ in air. This is confirmed by thermodynamic considerations [19] and Ellingham diagrams. In our experimental measurement conditions (T < 300 K), we assumed that 100% of cerium is Ce^{4+}. Therefore, the variation of the magnetic susceptibility (χ, expressed in emu) with the temperature is only linked with the modification of Pr4+/Pr3+ ratio and can be expressed per mol of Pr. The linear variation of the reciprocal magnetic susceptibility was plotted against temperature to extract the Curie constants (C) according to the Curie-Weiss law:

$$1/\chi = (T+ \theta p)/C \quad (1)$$

with χ = MH and θp is the Weiss temperature. The Pr^{4+}/Pr^{3+} ratio was estimated considering the theoretical effective moments of Pr^{4+} and Pr^{3+} cations (2.54 and 3.58 μB, respectively, CPr^{4+} = 0.806 emu K/mol, CPr^{3+} = 1.602 emu K/mol).

The reducibility of the mixed oxide was assessed by H_2-Temperature Programmed Reduction (TPR) experiments in a Thermoquest TPDRO 1100 equipped with a thermal conductivity detector (TCD). Around 200 mg of samples were first pre-treated at 500 °C (10 °C min^{-1}) for 1 h with 40 mL · min^{-1} of 5% O_2/He and then cooled-down under 5 vol.% O_2 in He to room temperature. TPR were recorded during heating ramps (10 °C · min^{-1}) in 40 mL · min^{-1} of 5% H_2/He up to 800 °C. The samples were maintained for 1 h at 800 °C.

O_2-Temperature Programmed Desorption (O_2-TPD) experiments were performed to investigate the oxygen evolution of the mixed oxides. The catalyst (around 200 mg) was placed in a U-shaped quartz reactor and was pretreated at 500 °C in O_2 (5 vol.% in He) for 1 h to clean (carbonate decomposition) and oxidize the surface. Then, it was cooled down to room temperature under the same atmosphere. After purging the system with He (15 min), O_2-TPD experiments were performed by heating up to 800 °C (10 °C · min^{-1}) in He (3 L h^{-1}). Online analysis of O_2 and CO_2 concentration was performed with a micro gas-chromatograph (SRA

3000) equipped with two TCD detectors, a molecular sieve and a Porapak Q column for O_2, CO, C_3H_8 and CO_2 analysis.

C_3H_8-TPR analysis were also performed to probe the reactivity of surface and bulk oxygen of ceria-based oxides. Around 100 mg of each oxide were pretreated using the same procedure as for O_2-TPD. C_3H_8-TPR experiments were operated with 2000 ppm C_3H_8 in He (10 L · h^{-1}) up to 600 °C (10 °C · min^{-1}). Online analysis of O_2, CO, CO_2 and C_3H_8 was performed with the same micro gas-chromatograph and with an on-line IR analyzer for CO_2 (Horiba). The carbon balance closure was calculated according as follow:

$$\text{C balance (\%)} = 100 \times \frac{3[C3H8]_i - (3[C3H8]_o + [CO2]_o + 2[C2H4]_o + 3[C3H6]_o)}{3[C3H8]_i} \times 100 \quad (2)$$

with $[C_3H_8]_i$ the inlet concentration of propane and $[CO_2]_o$, $[C_2H_4]_o$, $[C_3H_6]_o$ and $[C_3H_8]_o$ the outlet concentrations of CO_2, C_2H_4, C_3H_6 and C_3H_8. The C balance was found to be below 2% for all the catalysts below 550 °C. The C balance above 550°C exceeds 4%, most probably because side reactions such as cracking or reforming produce other compounds which are not analysed.

Ex situ scanning transmission electron microscopy (STEM) investigations were performed with an environmental transmission electron microscope (Ly-ETEM, ThermoScientific™ TITAN ETEM G2 80–300 kV) corrected for the aberrations of the objective lens. For this purpose, the samples were suspended in ethanol and transferred onto a carbon-covered Cu-grid. Bright Field TEM and Annular Dark Field-STEM (ADF-STEM) images were acquired at 300 kV under high vacuum.

The surface cationic sites were identified by using methanol as a probe molecule using *in-situ* IR measurements. The catalysts (24-28 mg) were pressed (~1 ton · cm^{-2}) into cylindrical pellets with a diameter of 16 mm. The pellets were pre-treated at 500 °C under pure O_2 for 20 min; after that, the samples were evacuated for 20 min at 500 °C. Then, the pellets were

cooled-down to room temperature and 133 Pa of methanol was introduced. After several minutes, methanol was evacuated. IR spectra was recorded after the evacuation. The same protocol was carried out after two successive reduction steps in 100 vol.% of H_2 at 400 °C for 30 min each one, followed by a gas evacuation before the methanol adsorption step.

2.3. Catalytic activity measurements

A mass of ca. 100 mg of each catalyst was placed in a U-shaped quartz reactor fitted with a fine-quartz fritted disk. The same pre-treatment as for O_2-TPD and C_3H_8-TPR was conducted before each catalytic test. These latter were performed using a 10 L · h^{-1} total gas flow, yielding a gas hourly space velocity of around 50 000 h^{-1} and 100 L · g_{cat}^{-1} · h^{-1}. A typical experiment consisted of 5 successive light-offs (LO) from 150 °C to 500 °C and 600 °C for CO and for C_3H_8, respectively (heating ramp: 2 °C · min^{-1}) with a 5 min plateau at the maximal temperature. The catalytic performance for CO oxidation was investigated during the two first LO, in lean (1910 ppm CO, 9 vol.% O_2 in He) and stoichiometric (2000 ppm CO, 1000 ppm O_2 in He) during the 1st and 2nd LO, respectively. The 3rd and 4th LO dealt with propane combustion, in lean (1960 ppm C_3H_8, 9 vol.% O_2 in He) and stoichiometric (2040 ppm C_3H_8, 1 vol.% O_2 in He) conditions, respectively. To check the stability of the catalysts, a 5th LO using identical conditions as the 1st one was conducted, which was found to be very similar (Fig. S2). These results demonstrate the catalytic properties stability of the ceria-based oxides in the operating conditions of this study, i.e. up to 600 °C in the reactive feed.

Reactants and products were analysed with the same gas micro-chromatograph and online CO_2 IR analyser as for C_3H_8-TPR experiments. Reactants were provided by Linde with certified standards C_3H_8 in He (8006 ppm), CO in He (4971 ppm) and O_2 (1 vol.% or 5 vol.% or 99.999%) that could be further diluted in He (99.999%). The conversions (X_i) of CO and C_3H_8 were calculated as follows:

$$X_{CO}(\%) = 100 * \frac{[CO]_{In} - [CO]_{Out}}{[CO]_{In}} \quad (3)$$

$$X_{C_3H_8}(\%) = 100 * \frac{[C_3H_8]_{In} - [C_3H_8]_{Out}}{[C_3H_8]_{In}} \quad (4)$$

The carbon balance closure was found to be below 5 vol.%. CO_2 was the predominant carbon-based product detected during propane oxidation catalytic tests. However, a small propylene and ethylene (max. 100 ppm) production was observed on all oxides above 350 °C and 450 °C, respectively.

3. Results and discussions

3.1. Structural and textural properties

The bulk chemical composition of the mixed oxides determined by ICP (Table 1) was closed to the theoretical one even if the Zr content was systemically slightly lower. All catalysts, annealed at 600 °C in air, crystallised in a single phase (Fig. S3) corresponding to the cubic fluorite-structure (SG: Fm-3m) except for CZ which also contains a minor contribution of the tetragonal phase (P42/nmc). Peaks of Pr-rich CZ (CZP45 and CZP47) were slightly shifted towards lower angles with respect of those of CZ and CZP8. This displacement was the result of a lattice parameter expansion. This could be also due to the lower Zr content in Pr-rich CZ compounds as the Zr^{4+} ionic radius (0.84 Å in coordination 8) is smaller than those of Ce^{4+} (0.99 Å) and Pr^{4+} (paler) cations. Furthermore, the expected presence of Pr^{3+} cations (1.12 Å) in CZP45 and CZP47 could also accentuate this peaks shift. The unit cell parameters of CZP45 and CZP47 are closed to those found in the literature for equimolar CP oxides calcined at 500 °C [12]. This parameter is expected to be lower with the zirconium content, explaining the smaller lattice parameter of CZ and CZP8 compared to that of CZP45 and CZP47 (Table 2). The presence of Pr^{3+} could also explain the slightly higher CZP8 lattice parameter compared to CZ. CZP45-LS exhibits the same lattice parameter (5.422 Å) as

CPZ47 despite a higher Zr rate and a larger one than CZP45-HS. All these results suggest a high Pr^{3+} content in CZP45-LS. Interestingly, the lattice parameters of Pr-rich CZP oxides slightly increase after grinding (Tab. S1). This increase is expected to be related to the enhancement of the amount of Pr^{3+} due to the grinding effect.

Table 2. Structural and textural properties of the oxides after grinding.

Catalysts	Average crystal size (nm)[a]	Lattice parameter (Å)[b]	S_{BET} (m^2/g)	Pore volume (cm^3/g)	Mean pore size (nm)	Pr^{4+}/Pr^{3+} ratio[c]
CZ	6(1)	5.387(1)	44	0.072	5	-
CZP8	6(1)	5.392(1)	52	0.073	4	-
CZP45-LS	7(1)	5.422(1)	14	0.022	5	30(1)/70(1)
CZP47	7(1)	5.422(1)	12	0.015	6	51(1)/49(1)
CZP45-HS[d]	8(1)	5.411(1)	52	0.096	6	80(1)/20(1)

[a] calculated using Scherrer's equation, [b] calculated for the cubic fluorite-structure, [c]from magnetic measurements, [d]calcined at 700°C with a modified method.

The average crystallite size was deduced from the determination of Lorentzian shape of diffraction peak and the Full Width at Half Maximum (FWHM) function of 2θ (Bragg) angle (Jana 2006 program and fundamental approach). The crystal sizes were estimated with Scherrer's equation using the (111) peak (Fig. 1) and found similar values of around 6 – 7 nm (Table 2) whatever the composition. However, as already observed [16], the insertion of a high Pr loading in the mixed oxides significantly decreases the specific surface area (Table 1). The S_{BET} values drop from around 44-52 $m^2 \cdot g^{-1}$ for CZ and CZP8 down to 12-14 $m^2 \cdot g^{-1}$ for CZP45-LS and CZP47. The lowest Zr content in Pr rich oxides most probably also contributes to the surface area decrease. The non-correlation between S_{BET} and crystal size r (in spherical approximation, r (nm) = $3/(\rho.S_{BET})$ where is the compound density) indicates that particles are not spherical and aggregation occurs limiting the pore size. High Pr loading decreases the intergranular porosity in line with the drop of the porous volume observed for

CZP45-LS and CZP47 (Table 1). Catalysts contain small mesopores (4-6 nm) in accordance with previous studies on CZP compounds [16].

In order to achieve CZP45 solids with higher surface area, the key step is the washing and centrifugation process in order to limit the ammonia content which contribute to limit the pore size and to decrease the surface area after annealing at T=700°C.

The modification of the preparation method, despite the higher calcination temperature (700 °C), strongly increases the pore volume and then the SSA of CZP45-HS to reach a value similar to that reported in a previous study [16]. We also notice that the grinding has a positive impact of the SSA of Pr-rich CZP with a low SSA (CZP45-LS and CZP47), increasing the pore volume (Table S1).

HR-TEM observations confirm that crystallites of CZP oxides are not spherical (Fig. 1). The size distribution of CZP8 crystallites is clearly narrower than that of Pr-rich CZP oxides. These latter contain a wide crystallite size distribution from around 4 up to 11 nm. In addition, they seem to stick to each other, highlighting a coalescence process triggered during the calcination at 600 °C, in agreement with their SSA. This is particularly evident for CZP47 such as on Fig. 4e where two crystallites have started to coalesce. FFT image analysis characterizes the presence of a fluorite cubic structure with d-spacing of 0.27 nm for the (200) plan (Fig. 1e, inset).

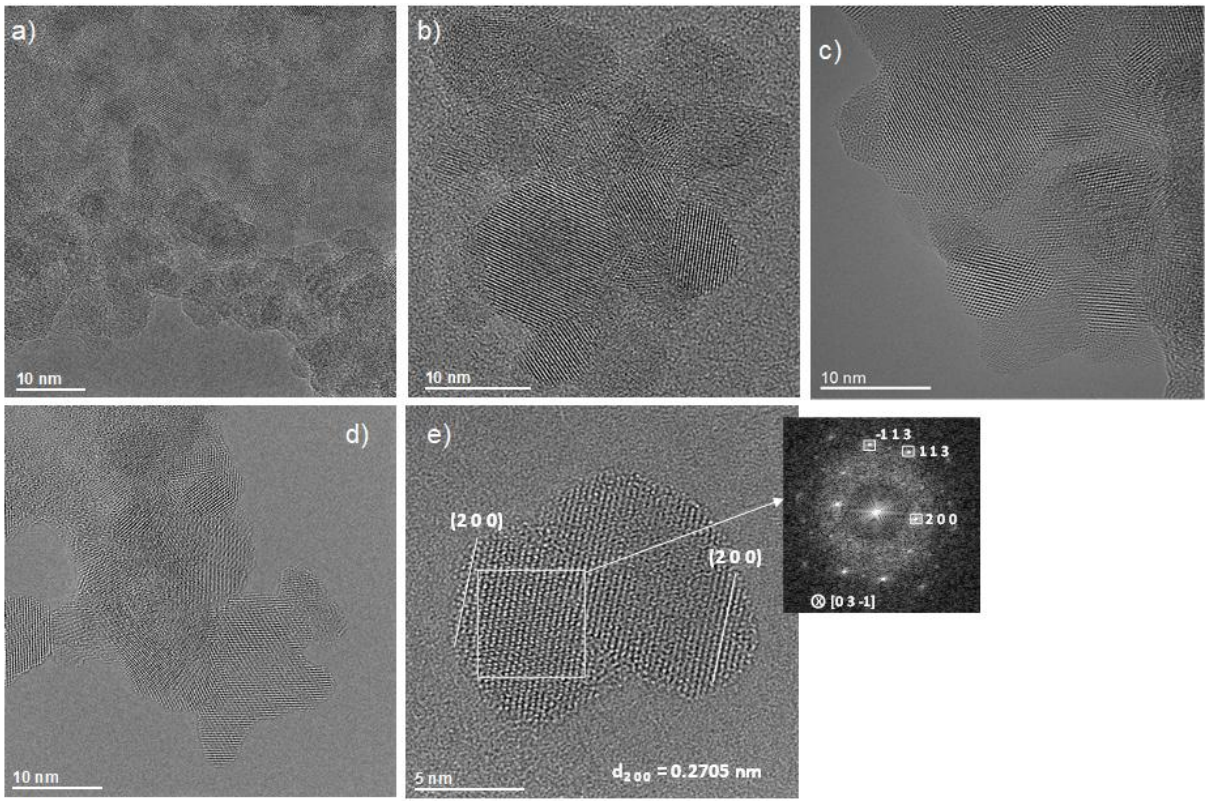

Fig. 1. Representative HRTEM micrographs of CZP oxides: a) CZP8, b) CZP45-LS, c) CZP45-HS and d) and e) CZP47. The inset in e) is the corresponding FFT (fast Fourier transform) diffraction image.

3.2. Magnetic measurements on Pr-rich CZP oxides

We have determined the bulk Pr^{4+}/Pr^{3+} ratio in air at low temperature (125-300 K) in the Pr-rich CZP oxides from their magnetic susceptibility (Table 2). As previously observed, the higher the Zr rate, the lower the Pr^{4+} content due to inductive effect. The more covalent Zr-O bonding induces a more ionic Pr-O bond, then stabilizing a larger content of Pr^{3+} in CZP45-LS compared to CZP47. This is also in line with the lattice parameter values (Table 2). The modified preparation method combined with a higher calcination temperature drastically decreases the Pr^{3+} concentration, which drops from 70% in CZP45-LS down to 20% on CZP45-HS, in accordance with lattice parameter values (Table 2). A similar Pr^{3+} rate (19 %) was found by magnetic measurements in previous CZP45 prepared by the same method and

calcined at the same temperature [19]. Therefore, two CZP45 oxides were successfully prepared showing different SSAs and Pr^{3+} concentrations. The high surface energy of CZP45-HS compared to CZP45-LS helps to stabilize a high content of less-coordinated Pr^{4+}-V_{O_2}- species at the surface. One should have to notice that the Pr^{4+}/Pr^{3+} cation ratio in CZP45-HS is close to that found in Pr_6O_{11}, 66% Pr^{4+} / 33% Pr^{3+}, the stable form of Pr binary oxide. The competition between Madelung lattice energy in the bulk and surface energy seems to tune the metastable Pr^{4+} content at the surface.

Taking into account what we observed by comparing the Pr^{4+}/Pr^{3+} cation ratio in CZP45-LS and -HS, surprisingly, we found that the mechanical grinding of the low-surface Pr-based oxides almost doubles the Pr^{3+} concentration (Table S1) in CPZ45-LS and CZP47, in good agreement with lower lattice parameters measured before grinding. This suggests that the high energy mechanical grinding process is reductive and not oxidative by stabilizing oxygen vacancies in Pr-rich CZP oxides, leading to the stabilization of more Pr^{3+} cations.

3.3. Reducibility

The H_2-TPR profile of CZ displays a non-symmetrical H_2 consumption peak centred at 580 °C linked to the reduction of Ce^{4+} cations [25], on the surface at low temperature and in the bulk above 500 °C (Fig. 2). The presence of Pr strongly improves the reducibility of the mixed oxides below 500 °C, in good agreement with previous studies [16,22,24]. A second non-symmetrical peak appears at around 460-480 °C attributed to Pr^{4+} reduction [25]. This latter clearly growths with the Pr content and becomes predominant for rich-CZP compounds. We recently proposed [16] that this Pr^{4+} reduction may occur in two successive steps, depending on the oxygen environment in the crystal network. According to the ionization energies, Pr^{4+} is less stable and more reducible than Ce^{4+}. The reducibility and oxygen

mobility in CZP oxides have been deeply analysed in our previous study [16]. We found that the combination of two rare earths (Ce/Pr) with various valences and polarizabilities with smaller and more polarizing Zr^{4+} cations, due to its lower ionic radius, contribute to a strong distortion of the oxygen tetrahedral sites. Therefore, the redox properties and oxygen mobility of CZP are related to the O/Zr local environments. For instance, as confirmed by magnetic measurements, the higher the Zr rate, the lower the Pr^{4+} content due to inductive effect and the higher the concentration of oxygen vacancies. The more covalent Zr-O bonding induces a more ionic Pr-O bond, then stabilizing a larger content of Pr^{3+} in CZP45-LS compared to CZP47. From our previous study, we have proposed that the most labile oxygen atoms, released below 400 °C during H_2-TPR, would be in Pr rich sites $OCe_1^{4+}Pr_2^{4+}Zr_1^{4+}$, while the second consumption peak at 460-480 °C would be linked to oxygen in the sites $OCe_1^{4+}Pr_1^{4+}Zr_2^{4+}$. This is in line with the apparent small temperature peak at 396 °C in the CZP8 TPR curve, which is present as a shoulder in the profiles of CZP45-LS and CZP47. The TPR profile of CZP45-HS is clearly shifted to lower temperatures probably because of its higher SSA, confirming that the low temperature reduction of all CZP compounds below 400 °C corresponds to the surface Pr^{4+} cations reduction. We also notice that the Pr^{4+} reduction in CZP47 seems to be slightly shifted to higher temperatures compared to CZP45. This could be attributed to the lower Zr^{4+} content linked with a lower SSA (Table 2). The peak area of the Ce^{4+} reduction at 580 °C decreases with the Pr content as expected, but it is still centred at the same temperature, indicating that the reduction of some Ce^{4+} cations is not affected by the presence of Pr in the lattice.

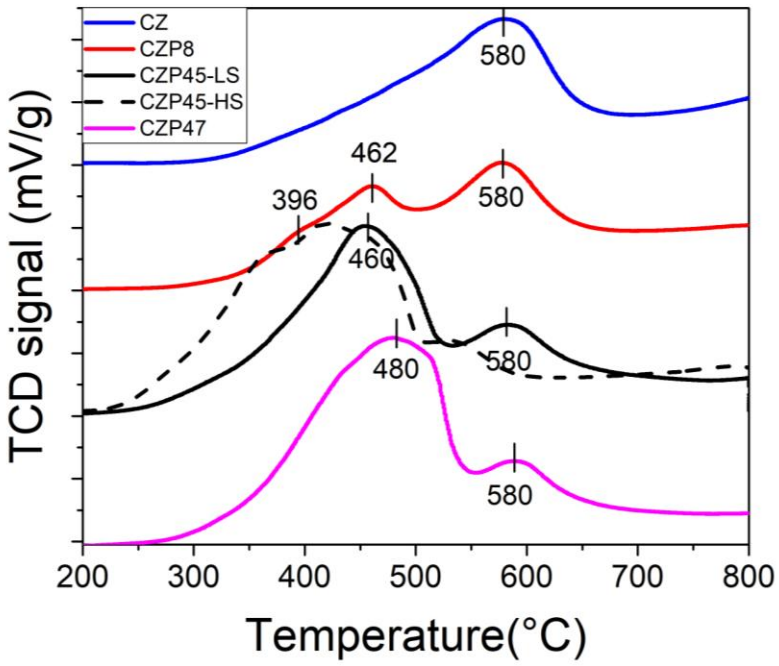

Fig. 2. H_2-TPR profiles of the catalysts.

Fig. 3 displays that the grinding has no impact on the TPR curve of CZ while significantly enhancing the intensity of the low temperature reduction of CZP oxides. This grinding effect is particularly pronounced for CZP47 since the increase of the low-temperature reduction peak is accompanied by a shift of around 50 °C to lower temperature. The grinding increases both the SSA and the Pr^{3+} loading (Tables 2 and S1) of the oxides. For instance, these two parameters are twice after grinding on CZP47. The grinding most probably enhances the intergranular porosity. A higher SSA promotes the H_2 adsorption while a higher Pr^{3+} loading is supposed to enhance the oxygen bulk mobility, leading to a greater low-temperature reducibility by keeping a high content of low-coordinated Pr^{4+}-V_{O_2} species at the surface.

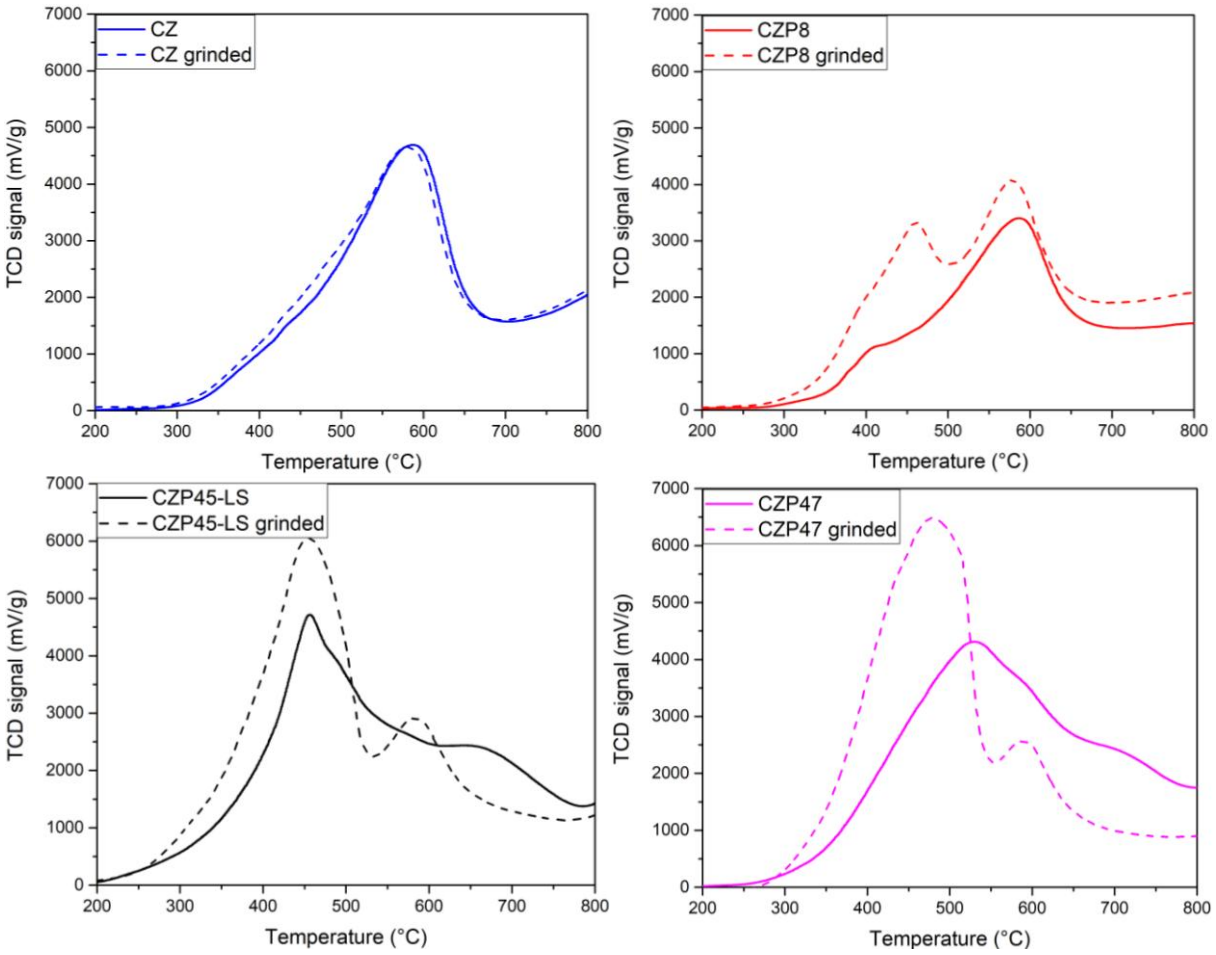

Fig. 3. H_2-TPR comparison profiles of the catalysts before and after grinding.

Table 3. H_2 consumption, concentrations of Ce^{4+}/Ce^{3+} and Pr^{4+}/Pr^{3+}, O loss and oxygen sub-stoichiometry (x) estimated from H_2-TPR.

Catalysts	H_2 uptake (µmol/g) up to 500 °C	Pr^{4+}/Pr^{3+} at 500°C	Temperature of full reduction of Pr^{4+} (°C)	Ce^{4+}/Ce^{3+} at 500 °C	H_2 uptake (µmol/g) up to 700 °C	Ce^{4+}/Ce^{3+} at 700 °C	%O loss 500/700 °C	x at 500/700°C
CZ	311	-	-	86/14	1057	53/47	2.5/8.3	0.049/0.166
CZP8	453	0/100	427	90/10	1130	56/44	3.6/8.9	0.071/0.168
CZP45-LS	887	0/100	350	64/36	1410	25/75	7.4/11.8	0.306/0.393
CZP45-HS	1196	0/100	395	91/9	1556	64/36	10/13	0.261/0.305
CZP47	851	0/100	363	90/10	1420	50/50	7.2/12	0.245/0.357

Table 3 confirms that the H_2 consumption below 500 °C is much higher for Pr-rich CZ oxides. Assuming predominant the reduction of Pr^{4+} vs. Ce^{4+} below 500 °C, an initial Ce^{4+} concentration of 100 °C and the initial Pr^{4+}/Pr^{3+} ratio defined by magnetic measurements, the Pr^{4+}/Pr^{3+} and Ce^{4+}/Ce^{3+} ratios were estimated at 500 °C from the H_2 consumption (Table 3). All Pr^{4+} cations of CZP oxides are reduced into Pr^{3+} below 500 °C. Furthermore, the overall reduction of Pr^{4+} cations, both on the surface and in the bulk, is achieved below 400 °C on Pr-rich CZP oxides, suggesting a very high oxygen bulk mobility. CZP45-LS exhibits the greatest rate of Ce^{3+} (36%) at 500 °C and the lowest temperature of full Pr^{4+} reduction in accordance with its high initial Pr^{3+} concentration. For the other oxides, the Ce^{3+} concentration at 500 °C is similar in the range 9-14%. This indicates a huge surface concentration of oxygen vacancies on CPZ45-LS which exhibits the highest non-stoichiometry values (x= 0.306, Table 3).

The overall H_2 consumption at 700 °C is still larger on Pr-rich CZ oxides, showing that their total reducibility is also higher. The reducibility of Pr-rich CZP compounds at 700 °C follows the rank: CZP45-LS (75% Ce^{3+}) > CZP47 (50% Ce^{3+}) > CZP45-HS (36% Ce^{3+}). Around 12-13% of oxygen atoms of Pr-rich CZP oxides were consumed by H_2 at 700 °C while the oxygen non-stoichiometry values are in the range 0.305-0.393. The total hydrogen consumption of Pr-rich CZP oxides is in the same range than reported in the literature for $Ce_{0.45}Pr_{0.55}O_{2-x}$ [6] (1396.5 µmol $H_2 \cdot g^{-1}$).

3.4. Oxygen evolution

The oxygen evolution of these oxides was investigated in He during TPD up to 800 °C (Fig. 4).

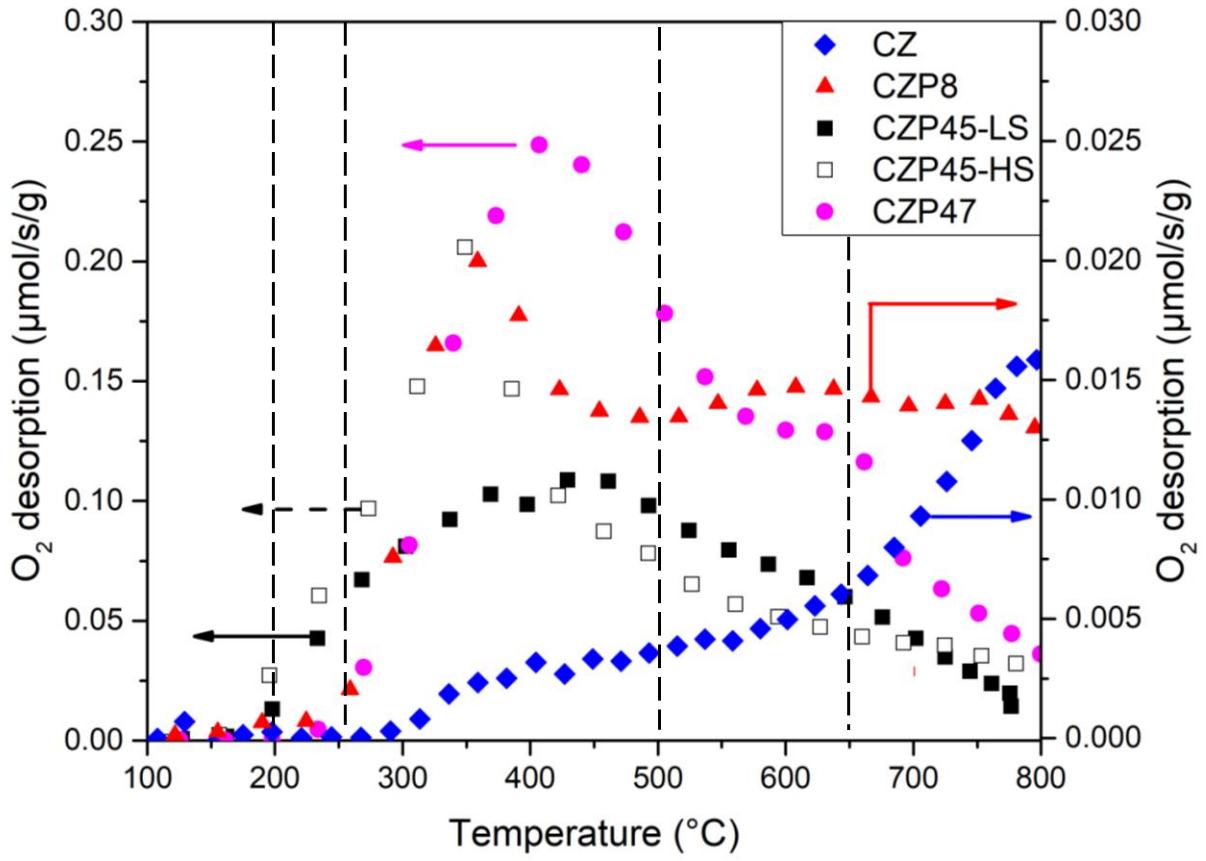

Fig. 4. O_2-TPD profiles of the catalysts.

The oxygen evolution rate of the Pr-free sample (CZ) is rather low (blue curve, right y axis in Fig. 4). A very small level of oxygen desorption starts from 300 °C and increases up to 600 °C to reach a peak centred at 800 °C. The insertion of a small Pr content in CZ promotes the oxygen evolution, as the O_2-TPD profile of CZP8 (red curve, right axis in Fig. 4) displays a peak centred at around 360 °C, most probably linked with the surface desorption of oxygen associated with the presence of Pr^{3+} cations and oxygen vacancies. The overall O_2 evolution of CZP8 is more than twice than that of CZ (Table 4). Considering a mean oxygen surface density of 21.7 µmol O $\cdot.m^{-2}$ in ceria-based oxides [26], the O_2 evolution of CZ and CZP8 only concerns surface oxygen species. These latter can be either adsorbed on surface oxygen vacancies during the pretreatment in O_2 at 500 °C or originate from the reduction of surface Pr^{4+} and Ce^{4+} cations during the TPD in He. The low temperature O_2 peak at 360 °C on CZP8 is most probably linked to the initial Pr^{3+} rate in the oxide surface, which triggers the

formation of surface oxygen vacancies, active sites for oxygen chemisorption. In our previous study, we have measured an initial Pr^{3+} concentration of 38% in a similar CZP10 oxide [16]. At high temperature, the surface reduction of Pr^{4+} and Ce^{4+} cations may occur in He from around 500 °C and 600 °C, respectively (Fig. 4). We estimated (Table 4) that 21% of Pr^{4+} cations were reduced during the TPD on CZP8.

The oxygen evolution rate of Pr-rich CZ oxides is much higher (Fig. 4, left y axis). The overall oxygen evolution of CZP47 is more than two order of magnitude higher than that of CZ (Table 4) and similar to values reported in the literature for CP oxides near to the equimolar Ce/Pr composition [2,12]. For CZP45-LS and CZP47, the O_2 evolution rate is maximal at 400 °C and starts from 200 °C and 250 °C for CZP45 and CZP47, respectively. The O_2 evolution is shifted to lower temperature for CZP45-HS with an onset and maximum temperature at 150 °C and 350 °C, respectively. The CZP47 oxygen evolution is larger than that of CZP45-LS and CZP45-HS below 500 °C (Table 4), indicating a better bulk oxygen mobility. The oxygen evolution of CZP45-LS and CZP47 not only concern surface species but at least 2 and 4 involved atomic layers, respectively. This highlights the high bulk oxygen mobility of these two oxides compositions, especially CZP47, which could be due, as proposed for $Ce_{0.45}Pr_{0.55}O_{2-x}$ [2], to the formation of oxygen vacancies channels in good agreement of high Pr^{3+} rates measured on these two oxides. Furthermore, by dividing by two the Zr rate on CZP47, the accessibility of Pr^{4+} at the surface was strongly enhanced. It is worth noting that the total amount of oxygen released (446 µmol $O_2 \cdot g^{-1}$) in He at 800 °C from CZP47 fairly corresponds to half of the H_2 consumption at 500 °C during TPR (425 µmol $H_2 \cdot g^{-1}$), then leading to the similar redox state of the oxide and the same oxygen loss. Considering the same assumptions as for TPR, we estimated the Pr^{4+}/Pr^{3+} ratios at 500 and 800 °C during TPD experiments in He (Table 4). Results confirm the high rates of Pr^{3+} on CZP45-LS and CZP47 in agreement with their huge surface and sub-surface oxygen mobility.

The desorption of CO_2 during O_2-TPD was also recorded (Fig. 5). As the oxides were pre-treated at 500 °C, the CO_2 production started above this temperature and corresponds to the decomposition of stable surface carbonates species. The desorption of CO_2 was found to be negligible on CZ. The formation of stable carbonate on the surface is clearly linked to the Pr content. On CZP47, the CO_2 desorption is maximal at 800 °C, highlighting strongly adsorbed carbonate species and an enhanced basicity of the Pr-rich oxide surface [27]. This basicity is indeed linked with the Pr^{3+} surface content. The quantification of the overall desorbed CO_2 up to 800 °C (Table 4) indicates that the surface Pr^{3+} concentration is the highest on CZP47 and CZP45-LS in agreement with magnetic measurements, TPR and XRD data. The surface basicity of CPZ47 is probably strengthened by a lower Zr^{4+} rate compared to CZP45. These results also suggest that a non-negligible part of the CZP47 and CZP45-LS surface is covered by carbonates even after a calcination step at 500 °C in oxygen. CZP45-HS desorbs a much less CO_2 quantity, in line with its lower Pr^{3+} concentration (Table 2).

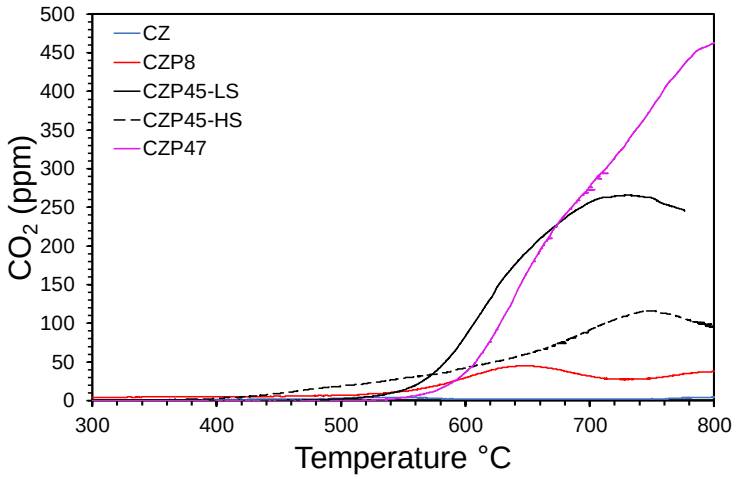

Fig. 5. Production of CO_2 as a function of temperature during O_2-TPD experiments.

To check the reversibility of the outstanding redox properties of CZP47, four successive O_2-TPD experiments were performed in He up to 500 °C with a 1 h step of re-oxidation at 500°C (temperature of the initial pretreatment) in 5vol% O_2/He (Fig. S4) after each TPD. We

obtained 4 fairly similar TPD profiles, demonstrating the full reversibility of the oxygen evolution (in He) and uptake (in O_2) in CZP47.

Table 4. O_2 evolution, percentage of oxygen released and of reduced Pr^{4+} cations.

Catalysts	Overall O_2 evolution µmol/m^2	µmol O_2/g up to 500 °C	Pr^{4+}/Pr^{3+} ratio at 500 °C	% O at 500 °C	µmol O_2/g up to 800 °C	% O at 800 °C	Pr^{4+}/Pr^{3+} ratio at 800 °C	Ce^{4+}/Ce^{3+} ratio at 800 °C	CO_2 / µmol/m²
CZ	0.37	4	-	-	21	0.3	-	98/2	-
CZP8	0.89	19	85/15	0.3	46	0.7	64/36	100/0	0.17
CZP45-LS	18	148	27/73	2.5	251	4.0	0/100	93/7	3
CZP45-HS	6.2	198	63/37	3.3	281	4.7	48/52	100/0	0.87
CZP47	40	256	28/72	4.3	446	7.6	0/100	87/13	5

3.5. Lattice oxygen reactivity

O_2-TPD experiments demonstrated that few % of oxygen in CZP45 and CZP47 (up to 4.3%) can be released below 500 °C in He and then could be available for catalytic reactions. To probe the reactivity of these oxygen species, C_3H_8-TPR experiments have been performed after a similar pretreatment as for O_2-TPD. We have chosen propane as a reductant as it is one of the most abundant unburned hydrocarbons in diesel and gasoline engine exhausts. The propane oxidation on ceria is supposed to proceed via a Mars and Van Krevelen (MvK) mechanism [28]. Propane deep oxidation requires active oxygen species that originate not only from the catalyst surface but also from the lattice via anionic mobility. Propane is supposed to remove surface lattice oxygen leading to the formation of oxygen vacancies and consequent replenishment of vacancies by gas phase oxygen. In addition, the cleavage of the first C-H bond of propane, which is the rate-limiting step), is energy demanding, leading to an activation energy of ca. 70-80 kJ/mol.

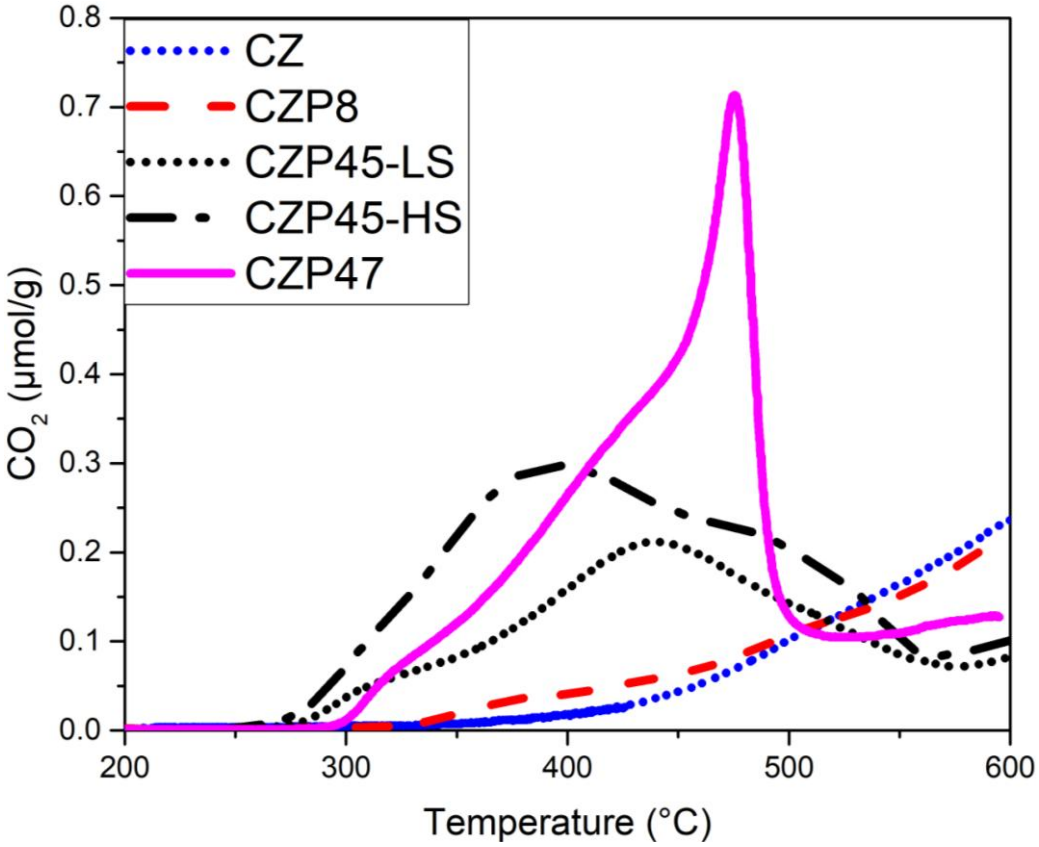

Fig. 6. C_3H_8-TPR profiles of the catalysts.

Fig. 6 displays the CO_2 production as a function of the temperature on the different catalysts during C_3H_8-TPR experiments. The CO_2 emission proves that propane is deeply oxidized by reactive oxygen species available on the different catalysts. Fig. S5 evidences that the CO_2 production matches with the propane consumption.

CZ and CZP8 show two similar C_3H_8-TPR profiles (Fig. 6) with an onset temperature of around 330-350 °C followed by a gradual increase of the CO_2 production with the temperature. We observed a slightly better CO_2 evolution on CZP8 between 350 and 450 °C in line with the O_2 evolution peak (Fig. 4) observed during O_2-TPD. The onset temperature of the CO_2 production is shifted to lower values on CZP45-LS, CZP45-HS and CZP47, demonstrating that oxygen species on these Pr-rich compounds can activate propane below 500 °C. On CZP45-LS and CZP45-HS, the propane oxidation starts even below 300 °C. Contrarily to CZ and CZP8, the C_3H_8-TPR profiles of Pr-rich CZP oxides display several CO_2

production peaks below 500 °C. The largest overall CO_2 production was observed on CZP47 in line with its enhanced oxygen evolution. In addition, the CZP47 profile exhibits an abrupt drop of the CO_2 production with a concomitant production of CO at 480 °C (Fig. S6). This can be explained by the consumption by propane of all the reservoir of active oxygen species in the oxide. From 480 °C, the lack of oxygen triggers side reactions such as reforming or cracking leading to the production of CO. Considering the stoichiometry of the propane combustion (5), the total CO_2 production at 500 °C (Table 5) of CZP47 and CPZ45-LS corresponds to a total Pr^{4+} reduction and a partial Ce^{4+} reduction of 19 and 8%, respectively. The CO_2 production of CZP45-HS is much higher below 400 °C than that of CZP47 and CZP45-LS. This could be due to its less surface carbonatation and a higher surface concentration of active sites to chemisorb and activate propane.

$$C_3H_8 + 5\ O_2 \rightarrow 3\ CO_2 + 4\ H_2O \qquad (5)$$

The ratio between the produced CO_2 during C_3H_8-TPR and the total oxygen evolution during O_2-TPD was also calculated. Table 5 shows that this ratio for Pr-rich CZP oxides is in a reasonable agreement but lower than the expected value corresponding to the stoichiometry of the propane oxidation reaction (CO_2/O_2 = 1.66). This probably because a part of the CO_2 formed during C_3H_8-TPR experiments is stored on the surface as carbonates. Nevertheless, all these results confirm that lattice mobile oxygen species are active for the propane oxidation.

Table 5. CO_2 production during C_3H_8-TPR experiments

Catalysts	CO_2 production up to 500 °C / µmol/g	Pr^{4+} /Pr^{3+} ratio at 500 °C	Ce^{4+}/Ce^{3+} ratio at 500 °C	CO_2 (up to 500 °C) / O_2[a]	CO_2 production up to 600 °C / µmol/g	CO_2 (up to 600 °C)/ O_2[a]
CZ	37	-	95/5	-	132	-
CZP8	51	33/67	100/0	-	142	-
CZP45-LS	154	0/100	92/8	1	210	1.42
CZP45-HS	288	11/89	100/0	1.45	368	1.85
CZP47	293	0/100	81/19	1.15	370	1.44

[a] Ratio between CO_2 (µmol/g) produced during C_3H_8-TPR (up to 500 °C or 600 °C) and O_2 (µmol/g) released up to 500 °C (Table 4) during O_2-TPD, the theoretical ratio according to propane combustion (5) stoichiometry is 1.66.

3.6. Methanol-FTIR measurements on Pr-rich CZP oxides

We chemisorb methanol as methoxy species on the surface of CZP45-LS, CZP45-HS and CZP47 to probe by using FTIR spectroscopy the Ce^{4+}, Ce^{3+} and Pr^{3+} cationic sites. The position of the n (OC) vibration of methoxy is very sensitive to the nature of the adsorption site (number of atoms, nature (Ce, Zr, Pr) and degree of oxidation). Due to their low SSA, the quantity of species adsorbed is very low, thus explaining their low absorbance during FTIR experiments.

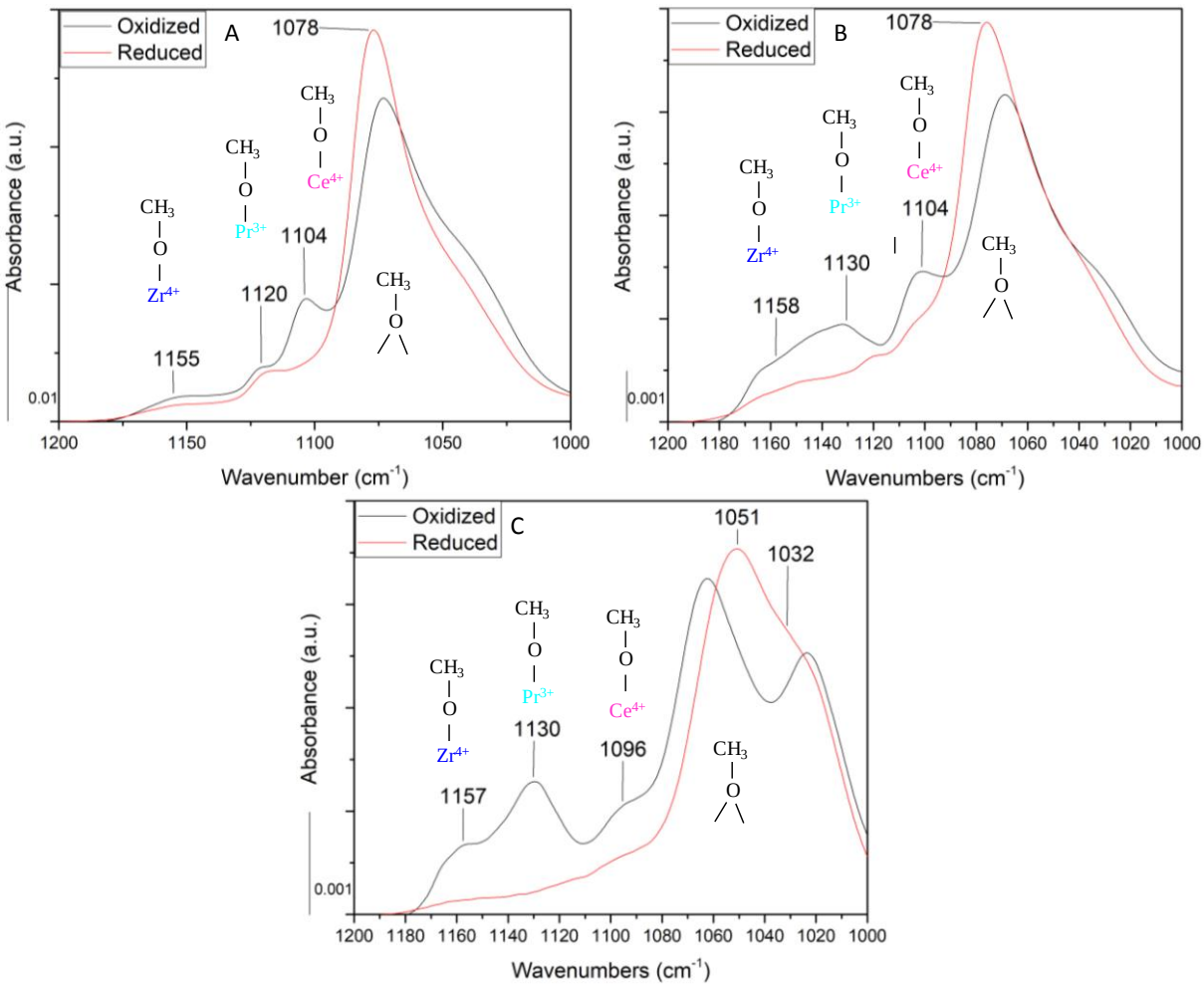

Fig. 7. FTIR spectra of methanol adsorbed at room temperature on: CZP after an oxidation step (500 °C 1h O_2) in black and after two successive reduction steps in red (at 400 °C 30 min in H_2). A) CZP45-HS, B) CZP45-LS and C) CZP47.

Fig. 7A shows the FTIR spectrum of methoxys adsorbed on cationic sites of CZP45-HS in the range of the ν(OC) vibrational mode, consequent to the dissociative adsorption of methanol. After having pretreated the sample by an oxidizing step, the spectrum shows bands at 1104 cm^{-1}, 1155 cm^{-1} and 1120 cm^{-1}, relative to methoxy linearly adsorbed on Ce^{4+} [29,30], Zr^{4+} [31], and Pr^{3+} [32] cations, respectively. The intense band at ~1075 cm^{-1} corresponds to bridged adsorption of methoxy species on both Ce, Zr and Pr cations (mainly Zr^{4+}) [29,32]. The small band at 1120 cm^{-1} confirms the presence of Pr^{3+} cations on the oxide even after an oxidation step at 500 °C. This band shifts to higher wavenumbers (from 1120 to 1130 cm^{-1})

on CZP45-LS and CZP47 (Figs 7B and C). This shift could be attributed [29] to the presence of Pr^{3+} cations surrounded by oxygen ions or oxygen vacancies. We have deconvoluted the FTIR spectra (Fig. S7) to estimate the area of each band. Table 6 gives the area ratios of bands relative to Ce^{4+} and Pr^{3+}. This ratio was found to be larger on CZP45-HS indicating a low concentration of Pr^{3+} cations vs. Ce^{4+} ones, in agreement with magnetic measurements. This ratio is lower than 1 for CZP45-LS and CZP47, confirming a high Pr^{3+} rate on these two oxides after an oxidation step. Spectra after H_2 reduction of CZP45-HS and LS show a decrease in the intensity of the band at 1104 cm^{-1} due to the reduction of Ce^{4+} and a growth of the band 1078 cm^{-1} relative to bridged methoxy (type II-A) species adsorbed on either on Pr^{3+} or Ce^{3+}cations formed after reduction [29,32]. The reduction of CZP47 also triggers the growth of the band II' at 1032 cm^{-1}, corresponding to bridged adsorption of methoxy species on both Ce^{4+} or Pr^{4+} cations surrounded by an oxygen vacancy [30,32], indicating a high surface concentration of oxygen vacancies on CZP47 after a reduction step at 400 °C.

Table 6. Area ratios of bands relative to Ce^{4+} and Pr^{3+} (FTIR spectra after an oxidation step).

Catalysts	Area ratio between the Ce^{4+} band at 1096-1104 cm^{-1} and the Pr^{3+} band at 1120-1130 cm^{-1}
CZP45-HS	2.3
CZP45-LS	0.45
CZP47	0.55

3.7. Catalytic activity measurements

The catalytic properties have been explored during five successive LOs for propane and CO oxidation, in lean and stoichiometric conditions as detailed in the experimental part. To check the stability and reproductivity of the catalytic properties, the first and last LO of a series of experiments were systemically performed under the same operating conditions (CO/O_2, lean

conditions). Fig. S2 displays that the catalytic performances recorded during these first and final LOs are identical for all samples, demonstrating the stability of the catalytic properties of the oxides.

Figs. 8, 9 and Table 7 summarize the catalytic performances of the oxides. The CO_2 production rates below 440 °C (Figs. 8B and 9B) indicate that the onset temperature is ca. 310-320 °C for all catalysts in both stoichiometric and lean conditions except for CZP45-HS which starts to be active from 290 °C. This onset temperature is similar to that recorded during C_3H_8-TPR experiments without any oxygen in the feed, confirming that the propane activation is the rate-determining step. Nevertheless, the catalytic performances of all the oxides are better in lean conditions than in stoichiometric ones. Values of T10 and T50 (temperatures at 10 and 50% conversion, respectively) are systematically higher in stoichiometric conditions, showing a positive impact of the oxygen partial pressure on the activity.

Catalytic performances of the oxides are, of course, SSAs dependent. By comparing oxides with similar SSAs in the range 44-52 $m^2 \cdot g^{-1}$ (CZ, CZP8 and CZP45-HS), conclusions can be clearly drawn on the promoting impact of Pr on the catalytic performances for propane oxidation. The higher the Pr^{3+} content in the different oxides, the higher the concentration of oxygen vacancies and then the catalytic activity. On the other hand, as observed during TPD experiments, a high Pr^{3+} surface concentration coupled with a low Zr^{4+} content leads to a strongly basic surface which is prone to carbonation. Accumulated carbonates on the surface can inhibit the accessibility of active sites. Values of T10 and T50 decrease with the Pr content in the oxides. For instance, T50 values in stoichiometric conditions drop from 546 °C for CZ down to 524 °C for CZP8 and 473 °C for CZP45-HS. However, despite a much lower SSA, T10 values of CZP45-LS are lower in both conditions than CZP8 and CZ, confirming

the key role of Pr cations. However, CZP47 exhibits the lowest catalytic performances. This could be due to an excessive carbonation of the surface (Fig. 5), cumulated with a low SSA. We have also compared the intrinsic catalytic rates of CO_2 production, expressed in mol/s/m², at 450 °C. Pr-rich CZP oxides show the highest catalytic activities, according to this classification: CZP45-LS > CZP47 > CZP45-HS >>CZP8 > CZ. For instance, the intrinsic catalytic of CZP45-LS is 3 to 5 times higher at 450 °C than on CZ and CZP8 in (Table 7) and 15 times larger than that reported in the literature for $Ce_{0.9}Zr_{0.1}O_2$ [33]. The apparent activation energy estimated below 440 °C (for low propane conversions) slightly decreases with the Pr loading in the oxide (Table 7). The apparent activation energy for propane oxidation on Pr-rich CZP oxides is ca. 87 ± 4 kJ/mol, in line with the cleavage of the first C-H bond of the hydrocarbon [28,34]. All these results emphasize the promoting effect of Pr^{4+}/Pr^{3+} pairs and the resulting concentration of oxygen vacancies on the catalytic activity for propane oxidation. A small propylene and ethylene production was observed both in lean and stoichiometric conditions above 350 °C and 450 °C, respectively (Figs. S8 and S9). Pr-rich oxides promote this formation of propylene and ethylene, which is, as expected, higher in stoichiometric conditions. This underlines that Pr-rich CZP oxides contain specific sites for the partial oxidation of propane. High concentrations of Pr^{3+} measured on CZP45-LS and CZP47 (Table 2) seem to promote this ethylene production.

The catalytic performances of the oxides for CO oxidation in both lean and stoichiometric conditions are reported in Figs. S10, S11 and in Table 8. CO oxidation starts from ca. 200 °C for all catalysts for both conditions. Performances are greater in lean conditions, showing the importance of the gaseous oxygen exchange on oxygen vacancies. Catalytic performances of CZ, CZP8 and CZP45-HS are very similar in line with their comparable SSAs. In the same way, low-SSA oxides (CZP45-LS and CZP47) are poorly active. The addition of Pr does not enhance the catalytic performances of ceria-zirconia

oxides for CO oxidation. Nevertheless, CZP45-LS shows the highest intrinsic rate at 300 °C, suggesting a higher surface concentration of active sites on this oxide. One can assume that oxygen vacancies produced by high rates of Pr^{3+} cations could promote the CO oxidation. However, the high intrinsic concentration of oxygen vacancies on CZP45-LS and CZP47 does not fully counter-balance their low SSAs. Furthermore, CO is a much more reducible agent than propane, and it can locally reduce Pr^{4+} and/or Ce^{4+} cations to operando form surface oxidation vacancies. In addition, CO oxidation occurs at much lower temperature than propane combustion in a temperature domain where the oxygen mobility seems to be not high enough.

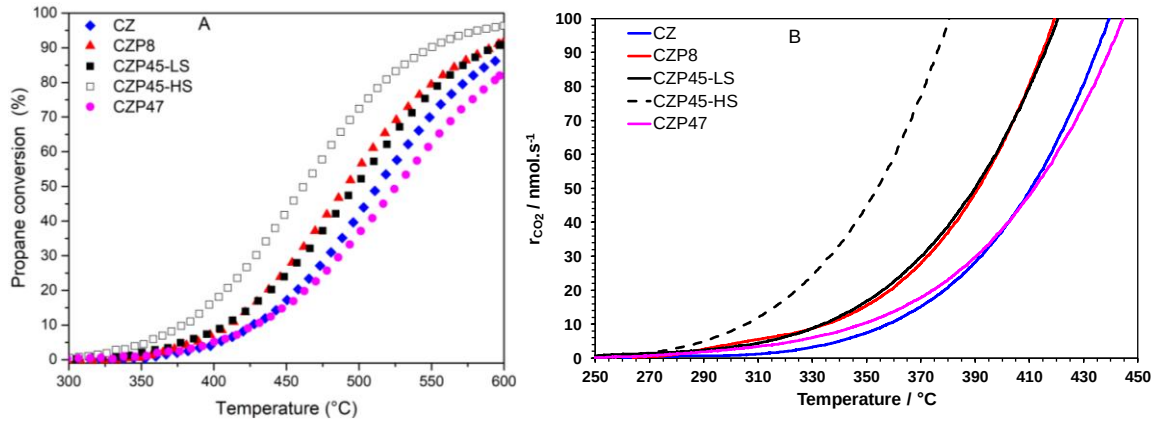

Fig. 8. Catalytic properties of mixed oxides for propane oxidation in lean condition (reactive mixture: C_3H_8/O_2: 2000 ppm / 9%): A) Variation of the propane conversion as a function of the temperature and B) Variation of the CO_2 production rate (below 450 °C).

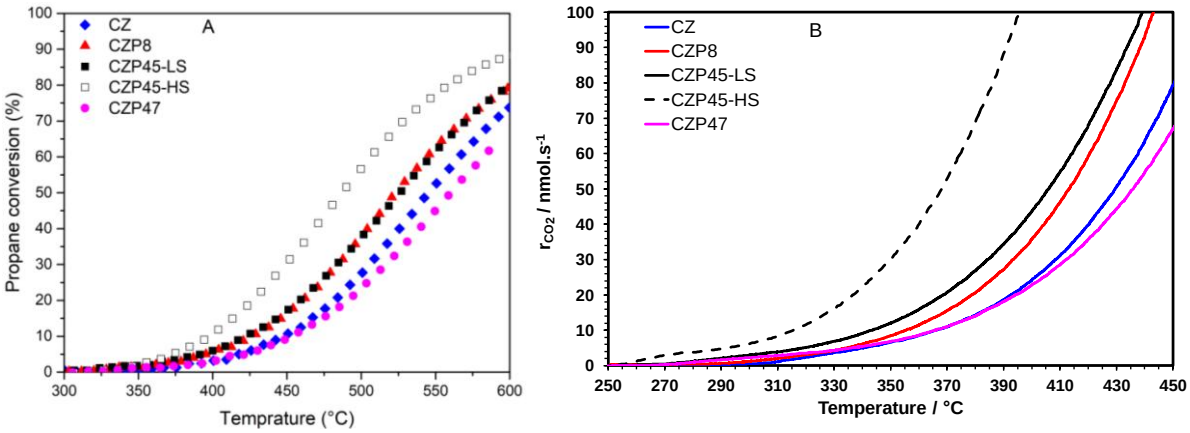

Fig. 9. Catalytic properties of mixed oxides for propane oxidation in stoichiometric condition (reactive mixture: C_3H_8/O_2: 2000 ppm / 1%): A) Variation of the propane conversion as a function of the temperature and B) Variation of the production rate of CO_2 (250-450 °C range).

Table 7. Catalytic activity parameters for propane oxidation.

Catalysts	Lean conditions				Stoichiometric conditions			
	T10	T50	r at 450°C nmol/s/m^2	Ea kJ/mol	T10	T50	r at 450 °C nmol/s/m^2	Ea kJ/mol
CZ	427	514	7.6	105 ± 4	450	546	4.8	93 ± 5
CZP8	413	492	9.4	91 ± 5	429	524	6.2	99 ± 5
CZP45-LS	408	497	33.5	90 ± 5	425	527	24	88 ± 4
CZP45-HS	381	463	16.9	88± 4	397	473	14	86 ± 4
CZP47	431	526	27.5	87 ± 4	453	560	17.1	86 ± 4

Table 8. Catalytic activity parameters for CO oxidation.

Catalysts	Lean conditions			Stoichiometric conditions		
	T10	T50	r at 300°C nmol/s/m^2	T10	T50	r at 300°C nmol/s/m^2
CZ	280	350	7.4	292	369	6
CZP8	277	342	7.5	295	373	4.3
CZP45-LS	292	368	17.2	310	398	10.6
CZP45-HS	280	351	7.8	287	372	6.1
CZP47	303	387	11.1	325	415	7.2

4. Conclusions

This study reports the textural, structural, redox, lattice oxygen reactivity and catalytic properties for propane and CO oxidation of Pr-rich (45 and 47.5 mol. %) cerium-zirconium-praseodymium (CZP) mixed oxides. We confirmed that Pr^{3+} cations can be stabilised on these oxides. Their concentration depends on the Zr content but also on the preparation method. For instance, a grinding step was found to strongly enhance the Pr^{3+} rate. Therefore, the Pr^{3+} rate

and the resulting oxygen vacancies concentration in CZP can be tuned according to the composition and the preparation method. High loadings of Pr in CZP mixed oxides enhance their low-temperature reducibility, oxygen mobility and catalytic activity for propane deep oxidation. For instance, the intrinsic catalytic rate of CZP45 ($Ce_{0.45}Zr_{0.10}Pr_{0.45}O_{2-x}$) is 5 times higher at 450°C than that of a ceria-zirconia oxide ($Ce_{0.70}Zr_{0.30}O_{2-x}$). Nevertheless, a minimal Zr^{4+} loading (10 mol. % such as in CZP45) seems to be necessary to counter-balance the high basicity of Pr^{3+} cations, which can cause a detrimental surface carbonation. Pr-rich CZP oxides are less relevant for CO oxidation which is mainly driven by the specific surface areas of the mixed oxides. Globally, all the oxides present a better performance for lean conditions, suggesting their possible role in diesel oxidation catalysts applications.

Acknowledgements

The French National Research agency 'Agence Nationale de la Recherche' (ANR), project CORAL (ANR-17-CE08-0022-02) is acknowledged for their financial support. The authors thank the CLYM for access to the Ly-ETEM.

References

[1] A. Trovarelli, Catal. Rev. - Sci. Eng. 38 (1996) 439–520.

[2] M.Y. Sinev, G.W. Graham, L.P. Haack, M. Shelef, J. Mater. Res. 11 (1996) 1960–1971.

[3] X. Wu, X. Wu, Q. Liang, J. Fan, D. Weng, Z. Xie, S. Wei, Solid State Sci. 9 (2007) 636–643.

[4] D. Devaiah, L.H. Reddy, S.E. Park, B.M. Reddy, Catal. Rev. - Sci. Eng. 60 (2018) 177–277.

[5] J. Abel, M. Lamirand-Majimel, J. Majimel, V. Bellière-Baca, V. Harlé, G. André, C. Prestipino, S. Figueroa, E. Durand, A. Demourgues, J. Chem. Soc. Dalt. Trans. 43 (2014) 15183–15191.

[6] A.D. Logan, M. Shelef, J. Mater. Res. 9 (1994) 468–475.

[7] T. Andana, M. Piumetti, S. Bensaid, N. Russo, D. Fino, R. Pirone, Appl. Catal. B Environ. 197 (2016) 125–137.

[8] T. Andana, M. Piumetti, S. Bensaid, L. Veyre, C. Thieuleux, N. Russo, D. Fino, E.A. Quadrelli, R. Pirone, Appl. Catal. B Environ. 226 (2018) 147–161.

[9] J. Giménez-Mañogil, N. Guillén-Hurtado, S. Fernández-García, X. Chen, J.J. Calvino-Gámez, A. García-García, Top. Catal. 59 (2016) 1065–1070.

[10] N. Guillén-Hurtado, J. Giménez-Mañogil, J.C. Martínez-Munuera, A. Bueno-López, A. García-García, Appl. Catal. A Gen. 590 (2020) 117339.

[11] C.K. Narula, L.P. Haack, W. Chun, H.W. Jen, G.W. Graham, J. Phys. Chem. B 103 (1999) 3634–3639.

[12] J.C. Martínez-Munuera, M. Zoccoli, J. Giménez-Mañogil, A. García-García, Appl. Catal. B Environ. 245 (2019) 706–720.

[13] K. Wu, L.D. Sun, C.H. Yan, Adv. Energy Mater. 6 (2016) 1–46.

[14] B. de Rivas, N. Guillén-Hurtado, R. López-Fonseca, F. Coloma-Pascual, A. García-García, J.I. Gutiérrez-Ortiz, A. Bueno-López, Appl. Catal. B Environ. 121–122 (2012) 162–170.

[15] I. Popescu, J.C. Martínez-Munuera, A. García-García, I.C. Marcu, Appl. Catal. A Gen. 578 (2019) 30–39.

[16] V. Frizon, J.M. Bassat, M. Pollet, E. Durand, J. Hernandez, K. Pajot, P. Vernoux, A. Demourgues, J. Phys. Chem. C 123 (2019) 6351–6362.

[17] M.F. Luo, Z.L. Yan, L.Y. Jin, M. He, J. Phys. Chem. B 110 (2006) 13068–13071.

[18] M. Rajendran, K.K. Mallick, A.K. Bhattacharya, J. Mater. Sci. 33 (1998) 5001–5006.

[19] S. Rossignol, C. Descorme, C. Kappenstein, D. Duprez, J. Mater. Chem. 11 (2001) 2587–2592.

[20] F. Colinot, F. Meunier, M. Daturi, Spectrosc. Eur. 21 (2009) 9–12.

[21] T. Y, S. T, M. Y, J. Appl. Electrochem. 14 (1984) 79–81.

[22] T. Andana, M. Piumetti, S. Bensaid, N. Russo, D. Fino, R. Pirone, Nanoscale Res. Lett. 11 (2016).

[23] S. Bensaid, M. Piumetti, C. Novara, F. Giorgis, A. Chiodoni, N. Russo, D. Fino, Nanoscale Res. Lett. 11 (2016) 494.

[24] M. Piumetti, T. Andana, S. Bensaid, D. Fino, N. Russo, R. Pirone, AIChE J. 63 (2017) 216–225.

[25] W. Wang, P. Lin, Y. Fu, G. Cao, Catal. Letters 82 (2002) 19–27.

[26] Y. Madier, C. Descorme, A.M. Le Govic, D. Duprez, J. Phys. Chem. B 103 (1999) 10999–11006.

[27] I. Tankov, B. Pawelec, K. Arishtirova, S. Damyanova, Appl. Surf. Sci. 258 (2011) 278–284.

[28] P.M. Heynderickx, J.W. Thybaut, H. Poelman, D. Poelman, G.B. Marin, J. Catal. 272 (2010) 109–120.

[29] C. Binet, M. Daturi, Catal. Today 70 (2001) 155–167.

[30] Z. Wu, M. Li, D.R. Mullins, S.H. Overbury, ACS Catal. 2 (2012) 2224–2234.

[31] M. Daturi, C. Binet, J. Lavalley, R. Sporken, Phys. Chem. Chem. Phys. 1 (1999) 5717–5724.

[32] LAHOUGUE M. Arnaud, Etude de Nouveaux Systèmes Catalytiques de Type Piège à NO x à Base de Terres Rares, 2008.

[33] P.M. Shah, A.N. Day, T.E. Davies, D.J. Morgan, S.H. Taylor, Appl. Catal. B Environ. 253 (2019) 331–340.

[34] K.A. Ledwa, L. Kępiński, M. Ptak, R. Szukiewicz, Appl. Catal. B Environ. 274 (2020) 1–10.

List of Tables

Figure captions

Fig. 7. FTIR spectra of methanol adsorbed at room temperature on: CZP after an oxidation step (500 °C 1h O_2) in black and after two successive reduction steps in red (at 400 °C 30 min in H_2). A) CZP45-HS, B) CZP45-LS and C) CZP47.

Fig. 8. Catalytic properties of mixed oxides for propane oxidation in lean condition (reactive mixture: C_3H_8/O_2: 2000 ppm / 9%): A) Variation of the propane conversion as a function of the temperature and B) Variation of the CO_2 production rate (below 450 °C).

Fig. 9. Catalytic properties of mixed oxides for propane oxidation in stoichiometric condition (reactive mixture: C_3H_8/O_2: 2000 ppm / 1%): A) Variation of the propane conversion as a function of the temperature and B) Variation of the production rate of CO_2 (250-450 °C range).